Quantitative susceptibility mapping of brain iron deposition in patients with type 2 diabetes mellitus

Jing Li
Beijing friendship Hospital
Qihao Zhang
Cornell University
Nan Zhang
Shandong University
Lingfei Guo (glfsci@163.com)
Shandong University https://orcid.org/0000-0002-4885-625X

Research article

Keywords: Type 2 diabetes mellitus, Magnetic resonance imaging, Quantitative susceptibility mapping, Iron deposition, Gray matter nucleus

Posted Date: May 17th, 2020

DOI: https://doi.org/10.21203/rs.3.rs-23880/v1

Abstract

Background Noninvasive quantitative susceptibility mapping (QSM) analysis was applied to assess brain iron deposition in the gray matter nucleus in type 2 diabetes mellitus (T2DM) patients and healthy elderly individuals.

Methods Thirty-two T2DM patients and thirty-two age- and gender-matched healthy controls (HCs) were enrolled in this research. All participants underwent brain magnetic resonance examinations. Twenty-three DM patients and twenty-six healthy controls received cognitive function assessments. Imaging data were collected with three-dimensional fast low-angle shot sequences to obtain magnitude and phase images; with preprocessed QSM data, ITK-SNAP helped to measure the susceptibility values reflecting the content of iron in the regions of interest (ROIs).

Results The study included thirty-two T2DM patients (20 males and 12 females; mean age of 61.09 ± 9.99 years) and 32 HCs (14 males and 18 females; mean age of 59.09 ± 9.77 years). These participants were age- and gender-matched, with no significant difference ($P > 0.05$). T2DM patients exhibited an obviously ($P < 0.05$) lower MoCA score (26.78 ± 2.35; normal standard, ≥ 27) and higher SCWT score (157 (128,188); HC, 123 (112,152)) than HCs. The mean susceptibility values in the left putamen and right putamen as well as dentate nucleus in the left thalamus appeared obviously higher in T2DM patients than in HCs ($P < 0.05$). In all participants, the susceptibility values in the left dentate nucleus were significantly higher than those in the right side ($P < 0.05$). The susceptibility values and cognitive assessment scores showed no obvious association ($P > 0.05$). However, an obvious correlation exists between the changes in the susceptibility values across hemispheres in the dentate nucleus and the putamen (left, $r = 0.439$, $P = 0.000$; right, $r = 0.260$, $P = 0.038$).

Conclusion T2DM patients showed increased iron deposition in the putamen, dentate nucleus and left thalamus. Cerebral iron deposition exacerbates cognitive decline in T2DM patients. Changes in susceptibility values in these regions are likely to be quantitative imaging markers of central nervous system injury in T2DM patients, and QSM may benefit their detection and evaluation.

Background

As a complicated metabolic disorder, diabetes mellitus (DM) mainly features hyperglycemia caused by insulin insufficiency and dysfunction. According to figures, approximately 425 million adults suffered DM in 2017 worldwide (1) (2). Type 2 diabetes mellitus (T2DM) is a long-term DM, and its symptoms include hyperglycemia, insulin resistance, and insulin deficiency, which accounts for the great majority of the diabetes burden, comprising 85% of DM patients. In T2DM, peripheral insulin resistance and insulin compensatory hypersecretion from the pancreatic islets are likely to decrease before the decrease in islet secretory function leads to several complications, such as neuropathy, nephropathy, atherosclerosis, and retinopathy (3).

Insulin resistance in the brain causes follow-up sequelae that possibly contribute to tau hyperphosphorylation and/or amyloid accretion. Insulin comes into play by distributing iron to neuronal tissue; however, the insulin-resistant state disrupts this process, and as a result, iron is overloaded in neurons and finally becomes detrimental (4). T2DM can impact diseases of the peripheral nervous system, and excessive iron could lead to lesions in the central nervous system. T2DM patients suffer cognitive deficits in memory, executive function, attention, visuospatial ability and deficits in other domains. It has been found that T2DM patients show poor performance on the cognitive scale, and their manifestation of neural slows and cortical atrophy increases (5). It has been proposed that the early onset of T2DM, weak glycemic control and the existence of microvascular and macrovascular complications can together result in cognitive impairment. T2DM can be used independently to measure the risk of Alzheimer's disease (AD), vascular dementia (VD) and mild cognitive impairment (MCI) (6).

Iron is an important auxiliary factor for the body's oxygen binding and transportation, energy and material metabolism, which can affect oxygen transportation, cell growth regulation, electron transport, and synthesis of DNA. If iron homeostasis is impaired, reactive oxygen species will be produced excessively, and apoptosis will occur (7) (8). In addition, as iron accumulates, protein will undergo misfolding and aggregation, resulting in different related diseases. Iron chelation therapy can reduce the overload of iron, which accordingly has the function of changing the glycemic control of T2DM individuals (9).

Based on an increasing number of studies regarding magnetic resonance imaging (MRI), brain iron overload can be seen in different neurodegenerative diseases (10) (11). Quantitative susceptibility mapping (QSM) is a newly found MRI approach that can help quantify materials with changing susceptibility and has been shown to provide a noninvasive quantitative analysis of brain iron deposition(12) (13) (14). In normal healthy people, iron content is different in various regions of brain tissue, and the iron content is high in deep gray matter nuclei, such as the globus pallidus, putamen, dentate nucleus, substantia nigra and red nucleus. The reasons for the differential regional distribution of brain iron may be related to the iron ions being involved in the synthesis of neurotransmitters and the various metabolic activities across regions and types of neurons. However, the association between cerebral iron accumulation and T2DM and iron distribution in vivo in patients with T2DM has not been completely elucidated. In this study, the noninvasive quantitative analysis QSM was performed to assess the deposition of brain iron in T2DM patients. To explore the differences between the patients with T2DM and healthy elderly individuals, QSM was used to evaluate and compare the deposition characteristics of iron in the gray matter nuclei in T2DM patients compared to healthy volunteers.

Methods

Participants

In the cross-sectional study, thirty-two T2DM patients (20 male; mean age, 61.09 ± 9.99 years; range, 41–73 years) and thirty-two age- and gender-matched healthy control volunteers (HCs) (14 male; mean age, 59.09 ± 9.77 years; range, 41–73 years) were enrolled from September 2018 to August 2019. All

participants were right-handed, and the patients met the diagnostic criteria of T2DM (15). Patients with the following conditions were excluded: organic brain lesions, such as cerebral apoplexy, brain tumors, brain trauma, etc.; a history of other mental illnesses; the existence of serious damage to the heart, liver, kidney and other organs; severe hypertension blood pressure that was not well controlled; severely impaired visual and auditory functions; and an MRI scan contraindication. This study obtained approval from the institutional review board of Shandong Medical Imaging Research Institute Affiliated to Shandong University. All participants were informed of the detailed experimental procedures and signed informed consent forms. Considering that the participants may have cognitive impairment, all subjects were invited to test their levels of cognitive function, and 49 people (23 T2DM patients and 26 HC) completed the questionnaire.

The Montreal Cognitive Assessment (MoCA) helped to globally assess cognitive functions (16, 17). The MoCA involves tests of visuospatial, verbal, and visual memory and attention and applies well to screening for cognitive impairment in T2DM patients. The study also paid attention to assessing different executive functions, such as inhibition, working memory and flexibility. In brief, the Rey auditory verbal learning test (AVLT) helped to assess verbal memory ability (18); the symbol digit modalities test (SDMT) for attention and information processing speed (19); the trail-making test (TMT) for attention, information processing speed, visual search and motor coordination (20); and the Stroop color-word test (SCWT) for interference (21). The test implementer was professionally trained and qualified and had no knowledge of the subject grouping.

Image acquisition

All subjects underwent MRI on a 3.0 T whole-body system (Magnetom Skyra, Siemens Healthcare, Erlangen, Germany), which has a 32-channel head coil. The obtained fluid attenuated inversion recovery, T2-weighted turbo-spin-echo, and diffusion-weighted images were considered for excluding individuals with any type of brain abnormalities. Ten echoes were used to perform a 3-dimensional (3D) rapid low-angle shot sequence for evaluating the changes in the susceptibility of the brain, and the parameters below were used to obtain magnitude as well as phase images. Echo time: 6.8–43.7 milliseconds (ms) with an interval of 4.1 ms; repetition time: 36 ms; flip angle: 15°; field of view: 195 × 195 × 240 mm^3; matrix size: 192 × 192 mm^2; and slice thickness: 2 mm. In addition, for obtaining the 3D T1-weighted structural images, the parameters below were applied to the rapid acquisition prepared under magnetization with a gradient echo sequence. Repetition time: 7.3 ms; echo time: 2.4 ms; flip angle: 9°; inversion time: 900 ms; shot interval: 1900 ms; field of view: 256 × 256 × 176 mm^3; matrix size: 256 × 256 mm^2; and slice thickness: 1 mm, an iso-voxel resolution of 1 mm^3 is finally yielded.

QSM preprocessing and quantitative analysis

The preprocessing of QSM original images conformed to the standard preprocessing steps. QSM was constructed from GRE data using Morphology Enabled Dipole Inversion With Automatic Uniform Cerebrospinal Fluid Zero (MEDI + 0) (22). The preprocessing and analysis of QSM images were conducted by virtue of a tool box together with a standardized algorithm based on Liu T et al. (23). A

nonlinear fitting was first performed regarding multiecho data for estimating the inhomogeneity of the magnetic field, and phase unwrapping guided under magnitude was then conducted (23). The projection was applied onto the dipole field to remove the background field. Finally, inverting the remaining file helped to calculate QSM through MEDI + 0 (24). The 3D T1WI and QSM images were coregistered to a magnitude image of the first echo obtained from the 3D GRE sequence of the same subject by using FSL software (FLIRT Linear Registration Tool, FMRIM Software Library, Oxford, England).

With the preprocessed data, the susceptibility values in the regions of interest (ROIs) were measured by ITK-SNAP (http://www.itksnap.org/pmwiki/, Version 3.8.0) software to reflect the iron content. The ROIs included the thalamus, caudate nucleus, putamen, pallidum, dentate nucleus, red nucleus, and substantia nigra. The ROIs of white matter were selected from frontal lobe subcortical white matter without T2WI/T2WI- FLAIR images. These regions were measured to take the mean value of both sides. Data from the left and right sides were separately recorded. The average QSM value in each ROI was then computed from all voxels overlapping with the corresponding label, and the boundaries of the ROIs were manually corrected on the QSM images (Fig. 1). The mean susceptibility value of the gray matter nucleus minus the mean susceptibility value of the white matter in the frontal lobe of the same patient was calculated; the same calculation method was used to record the susceptibility values in the left or right gray matter nuclei. Vessels were not included while drawing the ROIs. A senior neuroradiologist with 18 years of working experience performed the assessment of brain disease and pinpointed the ROI.

Statistical analysis

The Statistical Package for the Social Sciences (Version 21.0 for Windows; SPSS, Chicago, Ill) helped to carry out statistical analysis. A P value of < 0.05 was considered statistically significant. First, a descriptive analysis of thirty-two T2DM patients and thirty-two HCs was performed. The measurement data were represented in the form of the mean ± standard deviation, and the counting data were represented in the form of n (%) or median and interquartile range if the data did not obey the normal distribution. The chi-square test was applied to the comparison of count data. To compare the susceptibility values within a specific ROI or cognitive assessment scores between the patients with T2DM and HCs, the independent sample *t* test or the Mann-Whitney U test was used under the condition that data failed to obey the normal distribution. The correlations between susceptibility values and cognitive function scores were determined via Pearson or Spearman correlation analyses.

Results

Participant characteristics

Thirty-two patients with T2DM (20 males and 12 females, with a mean age of 61.09 ± 9.99 years) and 32 HCs (14 males and 18 females, with a mean age of 59.09 ± 9.77 years) were included in this study. These participants were age-, gender- and education-matched, showing no significant difference between groups ($P > 0.05$). Of the sixty-four participants, twenty-three patients with T2DM (11 males and 12

females; mean age, 64.65 ± 8.44 years) and twenty-six HCs (14 males and 12 females; mean age, 62.30 ± 6.13 years) received an assessment of cognitive function. Table 1 lists the clinical characteristics of the participants in the study.

Table 1
Clinical characteristics and assessment of cognitive function in the participants

Variables	T2DM (n = 23)	HC (n = 26)	Statistical value	P
gender(male)	11 (47.82%)	14 (53.84%)	0.177[a]	0.674
Age, years	64.65 ± 8.44	64.65 ± 8.44	1.650[b]	0.205
Education, years	11.34 ± 2.26	11.69 ± 2.40	0.515 [b]	0.609
Mo CA	26.78 ± 2.35	28.42 ± 0.64	3.237 [b]	0.003
ALVT Sum(N1-7) *	63.13 ± 14.88	65.03 ± 7.77	0.572 [b]	0.570
SDMT *	28.83 ± 12.68	35.73 ± 12.10	1.949 [b]	0.057
SCWT-Sum(A + B + C) [#]	157(128,188)	123(112,152)	-2.336[c]	0.020
TMT-Sum (A + B)[#]	260(212,365)	224(155,265.5)	-1.913 [c]	0.056

a, Chi-square test; b, independent sample t test; c, Mann-Whitney U test. *, the unit of scoring is number; [#], the unit of scoring is second. Sum, the sum of multiple subtests.

The MoCA and SCWT scores of the patients with T2DM and HC were significantly different (P < 0.05), and the patients with T2DM had lower MoCA scores (26.78 ± 2.35; normal standard ≥ 27) and higher SCWT scores (157 (128–188); HC, 123 (112–152)) than the HCs. The ALVT sum (N1-7), SDMT, and TMT-sum (A + B) scores of the patients with T2DM were not significantly higher than those of the HCs. The scores for each cognitive and behavioral assessment subindex in these tests and evaluations are shown in Table 1.

Susceptibility value analysis across ROIs

The comparison of susceptibility values from the patients with T2DM and the HCs is shown in Table 2 **and** Fig. 2. We found that T2DM patients presented obviously higher mean susceptibility values in the putamen and dentate nucleus than HCs, and the areas on the left and right sides of the brain showed the same difference (P < 0.05; Fig. 3a-b); the susceptibility values of the left thalamus appeared obviously higher in T2DM patients than in HCs (P < 0.05; Fig. 3c). The differences between the patients with T2DM and HCs were not significant in the right thalamus, pallidum, caudate nucleus, red nucleus and substantia nigra (P > 0.05); however, the susceptibility values in the patients with T2DM tended to be higher in most gray matter nuclei than those in the HCs. In the patients with T2DM and HCs, the susceptibility values on the left side of the dentate nucleus were significantly higher than those on the right side (P < 0.05), as shown in Table 3. The susceptibility values were not significantly correlated with the cognitive assessment score (P > 0.05). However, an obvious correlation existed between the changes in the

susceptibility values across hemispheres in the dentate nucleus and the putamen (r = 0.439, P = 0.000; right, r = 0.260, P = 0.038; Fig. 3d-e).

Table 2

The susceptibility value differences [ppb ($\times 10^{-9}$)] in gray matter nucleus

Variables	T2DM (n = 32)	HC (n = 32)	Statistical value	P
Thalamus	20.17 ± 19.30	12.25 ± 15.64	-1.803	0.076
Left-Thalamus	21.44 ± 22.31	10.02 ± 14.93	-2.406	0.019
Right-Thalamus	18.90 ± 21.96	14.48 ± 18.50	-0.871	0.387
Pallidum	198.78 ± 42.08	196.18 ± 43.51	-0.242	0.809
Left-Pallidum	199.78 ± 47.36	193.08 ± 43.70	-0.589	0.558
Right-Pallidum	197.78 ± 40.52	199.29 ± 44.58	0.142	0.887
Putamen	121.60 ± 25.37	96.43 ± 25.03	-3.994	0
Left-Putamen	121.38 ± 29.99	96.57 ± 27.52	-3.447	0.001
Right-Putamen	121.83 ± 26.65	96.30 ± 25.59	-3.908	0
Caudate nucleus	94.89 ± 44.18	88.29 ± 22.01	-0.756	0.452
Left-Caudate nucleus	90.43 ± 80.10	87.939 ± 22.86	-0.169	0.866
Right-Caudate nucleus	99.35 ± 21.07	88.64 ± 23.88	-1.901	0.062
Red nucleus	179.18 ± 36.59	168.55 ± 37.11	-1.153	0.253
Left-Red nucleus	177.65 ± 40.94	166.68 ± 38.31	-1.107	0.273
Right-Red nucleus	180.70 ± 37.36	170.41 ± 41.76	-1.038	0.303
Substantia nigra	179.93 ± 42.89	177.38 ± 40.58	-0.245	0.808
Left-Substantia nigra	182.34 ± 48.09	177.69 ± 43.22	-0.407	0.685
Right-Substantia nigra	177.51 ± 42.45	177.06 ± 41.53	-0.043	0.966
Dentate nucleus	129.96 ± 33.86	108.02 ± 41.98	-2.301	0.025
Left- dentate nucleus	131.79 ± 34.98	111.43 ± 45.61	-2.004	0.049
Right- dentate nucleus	128.14 ± 36.07	104.61 ± 39.85	-2.476	0.016
White Matter	-10.55 ± 10.73	-12.38 ± 10.46	-0.689	0.493
Left- White Matter	-12.19 ± 13.38	-11.31 ± 10.18	0.297	0.768
Right- White Matter	-8.92 ± 14.27	-13.45 ± 13.15	-1.321	0.191

Table 3

The susceptibility value differences [ppb ($\times 10^{-9}$)] between left and right in gray matter nucleus

Variables	Mean standard deviation	Standard error	95% confidence interval		t	P
			lower limit	upper limit		
Thalamus (Left-Right)	-0.96 ± 17.84	2.23	-5.41	3.49	-0.431	0.668
Pallidum (Left-Right)	-2.10 ± 21.53	2.69	-7.48	3.27	-0.782	0.437
Putamen (Left-Right)	-0.09 ± 21.76	2.72	-5.52	5.34	-0.034	0.973
Caudate nucleus (Left-Right)	-4.81 ± 55.21	6.90	-18.60	8.98	-0.697	0.488
Red nucleus (Left-Right)	-3.38 ± 28.91	3.61	-10.60	3.83	-0.937	0.352
Substantia nigra (Left-Right)	2.72 ± 26.97	3.37	-4.00	9.46	0.809	0.421
Dentate nucleus (Left-Right)	5.23 ± 19.28	2.41	0.41	10.05	2.17	0.034
White matter (Left-Right)	-0.56 ± 14.63	1.82	-4.21	3.09	-0.307	0.76
Left-Right, the susceptibility value in left region subtract the susceptibility value in right region.						

Discussion

In this study, we found significant differences in the regional susceptibility values in the putamen, dentate nucleus and thalamus between patients with T2DM and healthy elderly individuals. In iron-rich gray matter nuclei, the brain iron deposits in patients with T2DM have obviously increased in some gray nuclei in vivo. The increased iron content in these gray matter nuclei may be related to the iron ions influencing the synthesis of neurotransmitters and the various metabolic activities across regions and types of neurons. There were significant correlations between the changes in iron deposition across hemispheres in the dentate nucleus and the putamen. These brain regions contain important structures closely involved in cognitive, emotional, and motor functions, which suggests that the synergy of these changes may affect the neural pathways in the brain and impact the neural function of the brain. These findings suggest that increased iron deposition in the brain may be used for measuring the risk of the severity of brain injury in patients with T2DM. QSM can be used as a noninvasive quantitative analysis to assess brain iron deposition in patients with T2DM.

Iron is a fundamental requirement for most known life forms and is the richness trace element in the human body (25). Iron acts as a significant component of hemoglobin that participates in oxygen

transport. Iron in the nervous system can also affect catecholamine neurotransmitter metabolism and myelin formation. Hence, it is necessary to strictly regulate the metabolism of iron. Even so, excessive deposition of iron in the brain of the aged will easily lead to different kinds of neurodegenerative diseases (26). Therefore, studying and understanding the iron metabolism mechanism in the brain together with its regulation are of vital significance. (27). In normal healthy people, the deep gray matter nuclei have higher iron content and contain important structures closely involved in cognitive, emotional, and motor functions. This study consequently selected these areas as the research object.

We know that iron is an essential regulatory factor for glucose and lipid metabolism (28). As revealed by many studies, ferritin as the standard marker specific to iron stores can assist in increasing diabetes risk, such as insulin resistance (29) (30). Clinical studies have reported the direct association between iron overload in the human body and glucose intolerance, which can accordingly result in diabetes. Insulin resistance causes high permeability of the blood-brain barrier and induces a cognitive decrease in a mouse model induced by diabetic insulin resistance and in an AD model (31). Additionally, an overload of brain iron results in insulin resistance together with cognitive decrease in animal obesity models and human obesity models (32). In general, iron overload and iron deficiency can greatly affect the action of insulin as well as its relation to insulin resistance. As insulin resistance could trigger iron overload, we intended to identify the relationship between iron accumulation and central nervous system injury in patients with T2DM.

The dentate nucleus is the most lateral deep cerebellar nucleus and is rich in iron. The cerebellar vermis and roof of the fourth ventricle are adjacent to the dentate nucleus. A sagittal section through the dentate nucleus shows its serrated appearance (33). The dentate nucleus is capable of regulating fine control regarding voluntary movements, language, cognition, and sensory functions. Utilizing the dentatothalamic tract, the dentate nucleus sends output signals through the ipsilateral superior cerebral peduncle and then decussates to synapse in the contralateral ventrolateral (VL) thalamic nucleus. VL neurons send fibers to the precentral gyrus, premotor cortex, prefrontal gyri, posterior parietal areas, and basal ganglia, specifically the striatum (34) (35). Different parts of the striatum receive afferent input from various cortical regions, followed by projecting efferent output to the cortex through the thalamus (36). The anterior putamen links to the associative regions in the cortex, and the posterior portion links to the primary motor cortex as well as the supplementary motor area (37). We found significant changes in the susceptibility values in the putamen, dentate nucleus and left thalamus in the patients with T2DM. This may indicate that the increased iron deposition will cause damage to the gray matter nuclei, which may affect voluntary movements, cognition, language, and sensory functions.

The striatum plays a significant role in various brain functions, including language, motor learning and control, reward, cognitive functioning, and addiction through the functional cortico-striato-thalamocortical neural pathways (38) (39). Therefore, a pathologic state in the striatum can lead to a broad range of clinical manifestations from motor dysfunction, such as Parkinson’s disease, to various psychiatric disorders (40). Studies have shown that the dentate nucleus in the cerebellum leads to a tight disynaptic projection to the striatum. The basal ganglia, the cerebral cortex and the cerebellum together constitute

an integrated network, which undergoes topographical organization to ensure the interconnection among the motor, affective and cognitive domains of every node (35) (41). The iron deposition changes were significantly correlated across hemispheres in the dentate nucleus and the putamen, and the iron deposition in the left thalamus also increased. It was hinted that the synergy of these changes may potentially affect the cortico-striato-thalamocortical neural pathways and impact the neural function of the brain in patients with T2DM.

Regarding the deposition of brain iron in T2DM patients, previous study results regarding the content of iron in the pulvinar nuclei of patients who have neurodegenerative diseases are not consistent. A previous study investigated the deposition of iron in T2DM patients' brains and related cognitive impairments using QSM. The susceptibility of T2DM patients who did not undergo MCI and T2DM patients who underwent MCI remarkably increased in the left putamen. The susceptibility values in the left putamen can significantly affect the neuropsychological cognitive score (42). Our study showed similar results, which also suggested that there were obviously higher susceptibility values in the putamen in T2DM patients than in healthy elderly individuals. However, no correlations between susceptibility values and cognitive function scores were found, which may be due to the different research populations. T2DM patients were not divided into subgroups according to the degree of impairment in cognitive function. Some researchers have evaluated the effects of DM in patients with cognitive impairment using QSM. DM could lead to lower susceptibility changes in the pulvinar thalamus as well as hippocampus. The study showed region-specific changes in calcium deposition in DM subjects with cognitive impairment (43). Therefore, the reason for the difference between studies was the selection of patients with cognitive impairments with different independent risk factors in the previous study, and they did not make comparisons with healthy elderly individuals.

The comparison of the MoCA and SCWT scores between the patients with T2DM and healthy elderly individuals demonstrated that the patients with T2DM showed potential cognitive impairment compared to the healthy elderly individuals. MCI is generally considered to be the precursor of AD. The susceptibility values increased in the gray matter nuclei. However, a significant relationship between iron deposition and cognitive assessment scores was not found. It is suggested that the dentate nucleus-thalamus-putamen is the pivotal part of the cortico-striato-thalamocortical neural pathways that predict the conversion of MCI to AD in patients with T2DM. The increase in susceptibility values can be used as an important quantitative imaging marker. Previous studies have also shown that isolated putamen hemorrhage can lead to impaired frontal lobe function in patients, leading to attention-executive dysfunction (44); there are also task-related attentional and executive function disruptions involving the putamen of patients with multiple sclerosis clinically isolated syndrome (42, 45).

QSM acts as a new MRI approach that can quantify materials with changing susceptibility and has been shown to provide a noninvasive quantitative analysis of brain iron deposition (12) (13). It exhibits a stronger selectivity for iron compared with T2* relaxometry and can serve for data obtained via standard sequence acquisition that is available for a majority of commercial scanners. It acts as a useful computer algorithm for deriving values with sensitivity to the iron level from proper MRI data (14) (46). The iron

stored in ferritin, neuromelanin and hemosiderin in the brain tissue leads to high local magnetic and paramagnetic distortion (47). As a way to measure the level of brain iron, QSM boosts many advantages (14), which have been validated by MRI techniques sensitive to brain iron. It has been reported that brain iron burden under the measurement of the above techniques increases in AD subjects, with a positive relation to the amyloid-β burden and an inverse relation to cross-sectional cognitive performance in older and AD subjects (48) (49). In addition, the process of iron deposition in the brain during normal aging and neurodegenerative changes may cause neuronal damage through oxidative stress (42, 50). According to a review of the current literature, there are several potential reasons for cerebral iron deposition in patients with T2DM. Iron binds to amyloid-β to catalyze pro-oxidant radicals to be produced, thereby increasing the toxicity of peptide, which binds to tangles as well, leading to the formation of toxic radicals in neurons in a similar way (51). Synthetic amyloid-β intoxication in the mouse brain causes tau-dependent iron accumulation as well as cognitive impairment (52), which demonstrates that tau can mediate the effects of iron.

The study was a preliminary cross-sectional design study of brain iron changes in T2DM patients in a relatively small sample size. The iron deposition dynamics shall be observed, together with the examination of longitudinal levels of brain iron in T2DM patients in larger samples at different stages. It is necessary to perform a prospective study covering a large scale for determining the changes of magnetic susceptibility in certain regions as well as further exploring the potential mechanisms and the effect posed by iron deposition in gray matter nuclei pathology. Although automatic segmentation is the most appropriate method specific for imaging analysis based on previous studies, in this study, we use manual segmentation as the reference standard for complicated structures and try to use methods of whole-brain voxel analysis to make comparisons in further research.

Conclusion

In conclusion, T2DM patients showed increased iron deposition in the putamen, dentate nucleus and left thalamus. Cerebral iron deposition exacerbates the decline in cognitive function in patients with T2DM. The study finds that the deposition of iron in brain exhibits an association with T2DM, and the association may greatly affect the T2DM process. The change in susceptibility values in these regions is likely to be a quantitative imaging marker of central nervous system injury in T2DM patients, and QSM may remarkably benefit the detection and evaluation of T2DM.

Abbreviations

QSM, quantitative susceptibility mapping; T2DM, type 2 diabetes mellitus; HCs, healthy controls; ROIs, regions of interest; DM, diabetes mellitus; AD, Alzheimer’s disease; VD, vascular dementia; MCI, mild cognitive impairment; MRI, magnetic resonance imaging; MoCA, Montreal Cognitive Assessment; AVLT, rey auditory verbal learning test; SDMT, symbol digit modalities test; TMT, trail-making test; SCWT, stroop color-word test; 3D,3-dimensional; MEDI+0, Morphology Enabled Dipole Inversion With Automatic Uniform Cerebrospinal Fluid Zero; VL, contralateral ventrolateral

Declarations

Ethics approval and consent to participate: All study procedures were approved by the Ethical Committee of Shandong Medical Imaging Research Institute Affiliated to Shandong University. The patient legal guardian provided informed consent for publication.

Consent for publication: Written informed consent was obtained from the patient’s parent or guardian for publication of this case report and any accompanying images. A copy of the written consent is available for review by the Editor of this journal.

Availability of data and material: The datasets used and/or analysed during the current study are available from the corresponding author on reasonable request.

Competing interests: The authors declare no competing interests.

Funding: This work was supported by grants from National Natural Science Foundation of China (81800840), Technology Development Plan of Jinan (201301049, 201602206, 201907052) and Medical and Health Science and Technology Development Project of Shandong Province (2016WS0529).

Authors' contributions: J Li and LF Guo wrote the main manuscript text. QH Zhang prepared Figures 1-3. N Zhang prepared the clinical data and imaging data. LF Guo revised the main manuscript text. All authors reviewed the manuscript.

Acknowledgements: This manuscript has been edited and proofread by American Journal Experts.

References

1. Li R, Zhang Y, Rasool S, Geetha T, Babu JR. Effects and Underlying Mechanisms of Bioactive Compounds on Type 2 Diabetes Mellitus and Alzheimer's Disease. Oxidative medicine and cellular longevity. 2019;2019:8165707.
2. Nazir MA, AlGhamdi L, AlKadi M, AlBeajan N, AlRashoudi L, AlHussan M. The burden of Diabetes, Its Oral Complications and Their Prevention and Management. Open access Macedonian journal of medical sciences. 2018;6(8):1545-53.
3. Forbes JM, Cooper ME. Mechanisms of diabetic complications. Physiological reviews. 2013;93(1):137-88.
4. Medhi B, Chakrabarty M. Insulin resistance: an emerging link in Alzheimer's disease. Neurological sciences. 2013;34(10):1719-25.
5. McCrimmon RJ, Ryan CM, Frier BM. Diabetes and cognitive dysfunction. Lancet. 2012;379(9833):2291-9.

6. Moon Y, Han SH, Moon WJ. Patterns of Brain Iron Accumulation in Vascular Dementia and Alzheimer's Dementia Using Quantitative Susceptibility Mapping Imaging. J Alzheimers Dis. 2016;51(3):737-45.
7. Hubler MJ, Peterson KR, Hasty AH. Iron homeostasis: a new job for macrophages in adipose tissue? Trends Endocrinol Metab. 2015;26(2):101-9.
8. Apostolakis S, Kypraiou AM. Iron in neurodegenerative disorders: being in the wrong place at the wrong time? Rev Neurosci. 2017;28(8):893-911.
9. Swaminathan S, Fonseca VA, Alam MG, Shah SV. The role of iron in diabetes and its complications. Diabetes care. 2007;30(7):1926-33.
10. Daglas M, Adlard PA. The Involvement of Iron in Traumatic Brain Injury and Neurodegenerative Disease. Frontiers in neuroscience. 2018;12:981.
11. Ward RJ, Zucca FA, Duyn JH, Crichton RR, Zecca L. The role of iron in brain ageing and neurodegenerative disorders. Lancet. 2014;13(10):1045-60.
12. de Rochefort L, Liu T, Kressler B, Liu J, Spincemaille P, Lebon V, et al. Quantitative susceptibility map reconstruction from MR phase data using bayesian regularization: validation and application to brain imaging. Magnetic resonance in medicine : official journal of the Society of Magnetic Resonance in Medicine /. 2010;63(1):194-206.
13. Schweser F, Sommer K, Deistung A, Reichenbach JR. Quantitative susceptibility mapping for investigating subtle susceptibility variations in the human brain. NeuroImage. 2012;62(3):2083-100.
14. Wang Y, Spincemaille P, Liu Z, Dimov A, Deh K, Li J, et al. Clinical quantitative susceptibility mapping (QSM): Biometal imaging and its emerging roles in patient care. Journal of magnetic resonance imaging. 2017;46(4):951-71.
15. Alberti KG, Zimmet PZ. Definition, diagnosis and classification of diabetes mellitus and its complications. Part 1: diagnosis and classification of diabetes mellitus provisional report of a WHO consultation. Diabetic medicine. 1998;15(7):539-53.
16. Nasreddine ZS, Phillips NA, BÃ©dirian Vr, Charbonneau S, Whitehead V, Collin I, et al. The Montreal Cognitive Assessment, MoCA: A Brief Screening Tool For Mild Cognitive Impairment. Journal of the American Geriatrics Society. 2005;53(4):695-9.
17. Bergeron D, Flynn K, Verret L, Poulin S, Bouchard RW, Bocti C, et al. Multicenter Validation of an MMSE-MoCA Conversion Table. Journal of the American Geriatrics Society. 2017;65(5):1067-72.
18. Putcha D, Brickhouse M, Wolk DA, Dickerson BC, Alzheimers Dis Neuroimaging I. Fractionating the Rey Auditory Verbal Learning Test: Distinct roles of large-scale cortical networks in prodromal Alzheimer's disease. Neuropsychologia. 2019;129:83-92.
19. Benedict RH, DeLuca J, Phillips G, LaRocca N, Hudson LD, Rudick R. Validity of the Symbol Digit Modalities Test as a cognition performance outcome measure for multiple sclerosis. Multiple sclerosis. 2017;23(5):721-33.
20. Wei M, Shi J, Li T, Ni J, Zhang X, Li Y, et al. Diagnostic Accuracy of the Chinese Version of the Trail-Making Test for Screening Cognitive Impairment. Journal of the American Geriatrics Society.

2018;66(1):92-9.
21. Scarpina F, Tagini S. The Stroop Color and Word Test. Frontiers in Psychology. 2017;8:557.
22. Liu Z, Spincemaille P, Yao Y, Zhang Y, Wang Y. MEDI+0: Morphology enabled dipole inversion with automatic uniform cerebrospinal fluid zero reference for quantitative susceptibility mapping. Magnetic resonance in medicine : official journal of the Society of Magnetic Resonance in Medicine /. 2018;79(5):2795-803.
23. Liu T, Surapaneni K, Lou M, Cheng L, Spincemaille P, Wang Y. Cerebral microbleeds: burden assessment by using quantitative susceptibility mapping. Radiology. 2012;262(1):269-78.
24. Liu J, Liu T, de Rochefort L, Ledoux J, Khalidov I, Chen W, et al. Morphology enabled dipole inversion for quantitative susceptibility mapping using structural consistency between the magnitude image and the susceptibility map. NeuroImage. 2012;59(3):2560-8.
25. Aisen P, Enns C, Wessling-Resnick M. Chemistry and biology of eukaryotic iron metabolism. The international journal of biochemistry & cell biology. 2001;33(10):940-59.
26. Thirupathi A, Chang Y-Z. Brain Iron Metabolism and CNS Diseases. Advances in experimental medicine and biology. 2019;1173:1-19.
27. Hare D, Ayton S, Bush A, Lei P. A delicate balance: Iron metabolism and diseases of the brain. Frontiers in aging neuroscience. 2013;5:34.
28. Chung JY, Kim H-S, Song J. Iron metabolism in diabetes-induced Alzheimer's disease: a focus on insulin resistance in the brain. BioMetals. 2018;31(5):705-14.
29. Cho M-R, Park J-K, Choi W-J, Cho AR, Lee Y-J. Serum ferritin level is positively associated with insulin resistance and metabolic syndrome in postmenopausal women: A nationwide population-based study. Maturitas. 2017;103:3-7.
30. Krisai P, Leib S, Aeschbacher S, Kofler T, Assadian M, Maseli A, et al. Relationships of iron metabolism with insulin resistance and glucose levels in young and healthy adults. European journal of internal medicine. 2016;32:31-7.
31. Takechi R, Lam V, Brook E, Giles C, Fimognari N, Mooranian A, et al. Blood-Brain Barrier Dysfunction Precedes Cognitive Decline and Neurodegeneration in Diabetic Insulin Resistant Mouse Model: An Implication for Causal Link. Frontiers in aging neuroscience. 2017;9:399.
32. Fernández-Real JM, Manco M. Effects of iron overload on chronic metabolic diseases. The lancet. 2014;2(6):513-26.
33. Bond KM, Brinjikji W, Eckel LJ, Kallmes DF, McDonald RJ, Carr CM. Dentate Update: Imaging Features of Entities That Affect the Dentate Nucleus. American journal of neuroradiology : AJNR. 2017;38(8):1467-74.
34. Dum RP, Strick PL. An unfolded map of the cerebellar dentate nucleus and its projections to the cerebral cortex. Journal of neurophysiology /. 2003;89(1):634-9.
35. Bostan AC, Strick PL. The basal ganglia and the cerebellum: nodes in an integrated network. Nature reviews. 2018;19(6):338-50.

36. Haber SN. The primate basal ganglia: parallel and integrative networks. Journal of chemical neuroanatomy. 2003;26(4):317-30.
37. Alexander GE, DeLong MR, Strick PL. Parallel organization of functionally segregated circuits linking basal ganglia and cortex. Annual review of neuroscience. 1986;9:357-81.
38. Koikkalainen J, Hirvonen J, Nyman M, Lötjönen J, Hietala J, Ruotsalainen U. Shape variability of the human striatum--Effects of age and gender. NeuroImage. 2007;34(1):85-93.
39. Fazl A, Fleisher J. Anatomy, Physiology, and Clinical Syndromes of the Basal Ganglia: A Brief Review. Seminars in pediatric neurology. 2018;25:2-9.
40. Uono S, Sato W, Kochiyama T, Kubota Y, Sawada R, Yoshimura S, et al. Putamen Volume is Negatively Correlated with the Ability to Recognize Fearful Facial Expressions. Brain topography. 2017;30(6):774-84.
41. Hintzen A, Pelzer EA, Tittgemeyer M. Thalamic interactions of cerebellum and basal ganglia. Brain Struct Funct. 2018;223(2):569-87.
42. Yang QF, Zhou LN, Liu C, Liu DH, Zhang Y, Li C, et al. Brain iron deposition in type 2 diabetes mellitus with and without mild cognitive impairmentan in vivo susceptibility mapping study. Brain Imaging and Behavior. 2018;12(5):1479-87.
43. Park M, Moon W-J, Moon Y, Choi JW, Han S-H, Wang Y. Region-specific susceptibility change in cognitively impaired patients with diabetes mellitus. PloS one. 2018;13(10):e0205797.
44. Kokubo K, Suzuki K, Hattori N, Miyai I, Mori E. Executive Dysfunction in Patients with Putaminal Hemorrhage. Journal of Stroke & Cerebrovascular Diseases. 2015;24(9):1978-85.
45. Tortorella C, Romano R, Direnzo V, Taurisano P, Zoccolella S, Iaffaldano P, et al. Load-dependent dysfunction of the putamen during attentional processing in patients with clinically isolated syndrome suggestive of multiple sclerosis. Multiple Sclerosis Journal. 2013;19(9):1153-60.
46. Wang Y, Liu T. Quantitative susceptibility mapping (QSM): Decoding MRI data for a tissue magnetic biomarker. Magnetic resonance in medicine : official journal of the Society of Magnetic Resonance in Medicine /. 2015;73(1):82-101.
47. Bilgic B, Pfefferbaum A, Rohlfing T, Sullivan EV, Adalsteinsson E. MRI estimates of brain iron concentration in normal aging using quantitative susceptibility mapping. NeuroImage. 2012;59(3):2625-35.
48. Steiger TK, Weiskopf N, Bunzeck N. Iron Level and Myelin Content in the Ventral Striatum Predict Memory Performance in the Aging Brain. The journal of neuroscience : the official journal of the Society for Neuroscience. 2016;36(12):3552-8.
49. van Rooden S, Buijs M, van Vliet ME, Versluis MJ, Webb AG, Oleksik AM, et al. Cortical phase changes measured using 7-T MRI in subjects with subjective cognitive impairment, and their association with cognitive function. NMR in biomedicine. 2016;29(9):1289-94.
50. Carocci A, Catalano A, Sinicropi MS, Genchi G. Oxidative stress and neurodegeneration: the involvement of iron. Biometals. 2018;31(5):715-35.

51. Smith MA, Harris PL, Sayre LM, Perry G. Iron accumulation in Alzheimer disease is a source of redox-generated free radicals. PNAS : Proceedings of the National Academy of Sciences of the United States of America. 1997;94(18):9866-8.
52. Li X, Lei P, Tuo Q, Ayton S, Li Q-X, Moon S, et al. Enduring Elevations of Hippocampal Amyloid Precursor Protein and Iron Are Features of β-Amyloid Toxicity and Are Mediated by Tau. Neurotherapeutics. 2015;12(4):862-73.

Figures

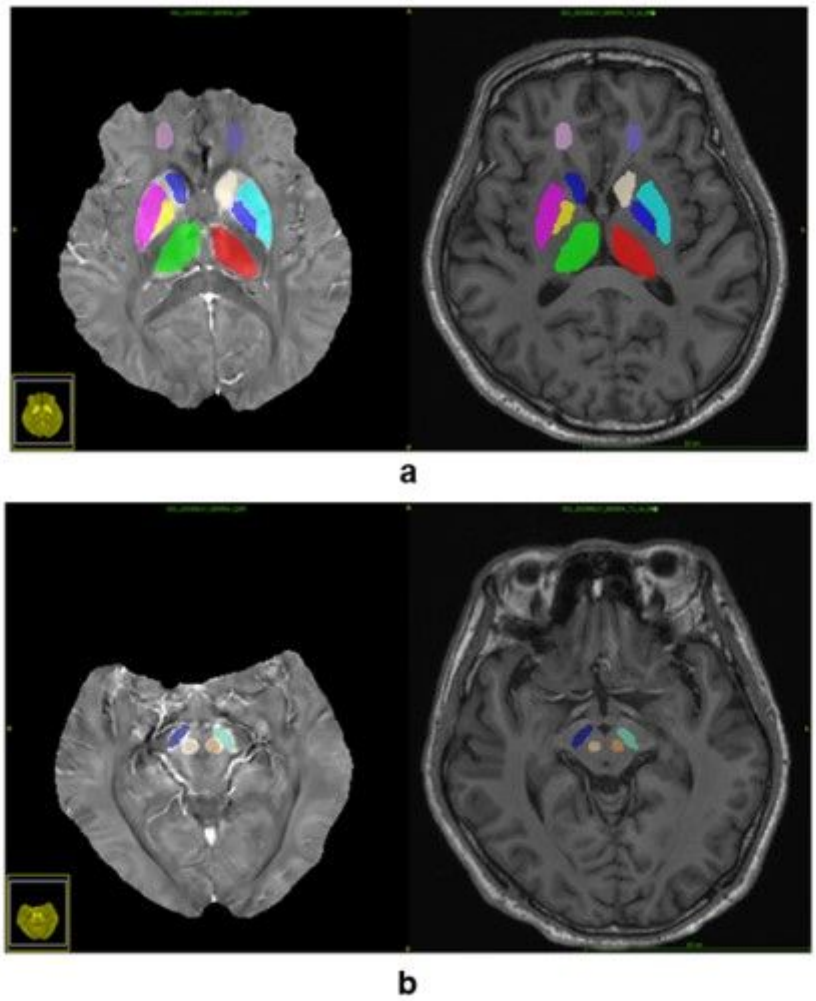

Figure 1

ROI sketch diagram. The 3D T1WI and QSM images were co-registered to a magnitude image of the first echo acquired from the 3D GRE sequence of the same subject by using FSL software. The gray matter nuclei and the frontal white matter (ROIs larger than 150 voxels) were drawn entirely by hand. The average QSM value in each ROI was then computed from all voxels overlapping with the corresponding label.

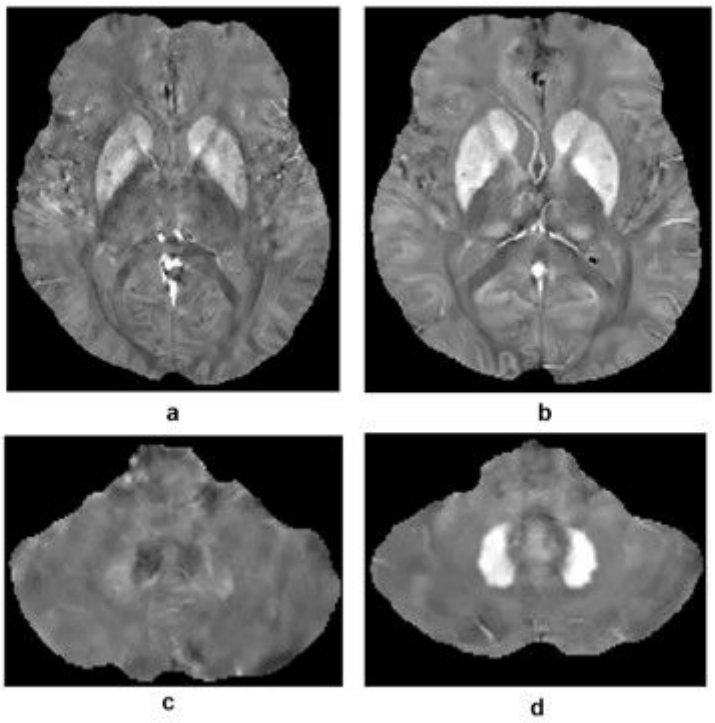

Figure 2

Brain susceptibility value differences between the patients with T2DM and HCs. (a, c), Healthy elderly individual; male; 71 years of age. (b, d) Patients with T2DM; male; 60 years of age.

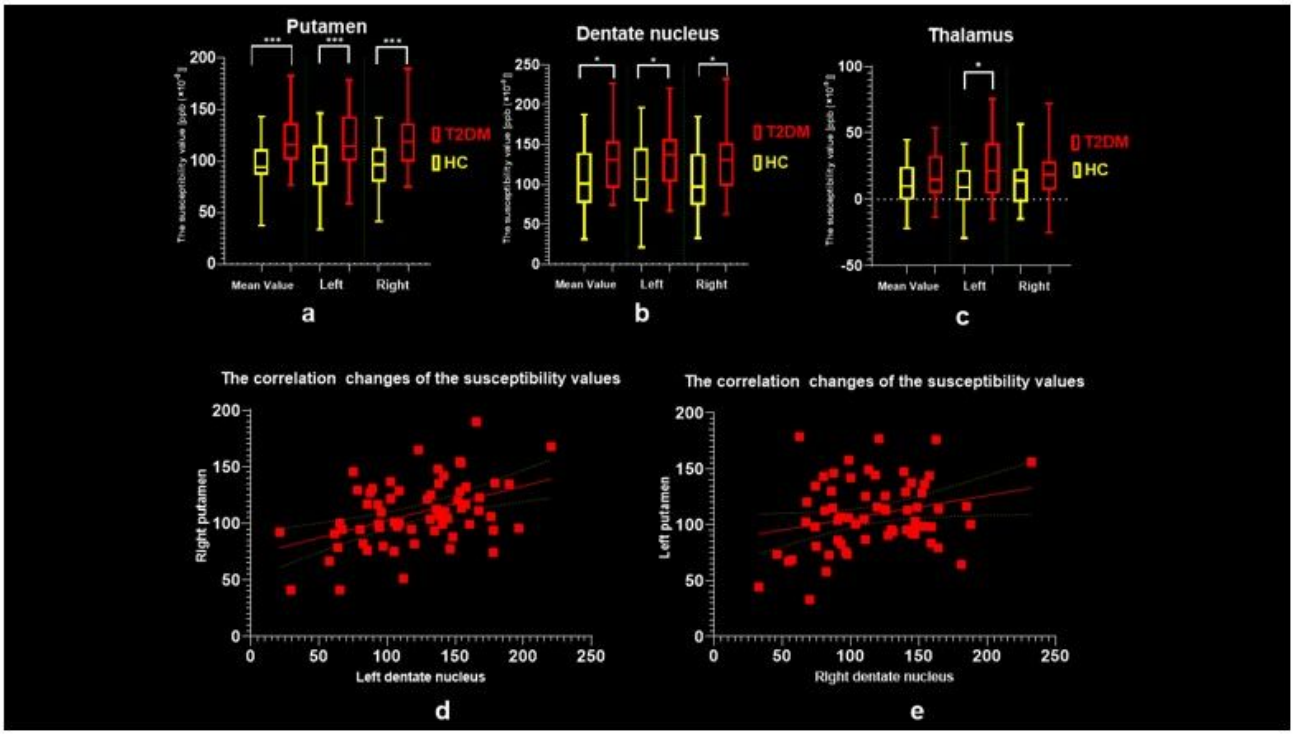

Figure 3

The susceptibility value [ppb (×10-9)] differences between the patients with T2DM and HCs in the putamen, dentate nucleus and thalamus. The correlation between changes in susceptibility values across hemispheres in the dentate nucleus and the putamen.